ACS APPLIED ENERGY MATERIALS

Article

Cite This: ACS Appl. Energy Mater. 2020, 3, 558−564

www.acsaem.org

On the Germanium Incorporation in $Cu_2ZnSnSe_4$ Kesterite Solar Cells Boosting Their Efficiency

Maurizio Ritzer,[*,†] Sven Schönherr,[†] Philipp Schöppe,[†] Wolfgang Wisniewski,[‡] Sergio Giraldo,[§] Galina Gurieva,[∥] Andreas Johannes,[⊥] Christian T. Plass,[†] Konrad Ritter,[†,#] Gema Martínez-Criado,[▽] Susan Schorr,[∥,○] Edgardo Saucedo,[§] Carsten Ronning,[†] and Claudia S. Schnohr[†,#]

[†]Institut für Festkörperphysik, Friedrich-Schiller-Universität Jena, Max-Wien-Platz 1, 07743 Jena, Germany

[‡]Centre for Functional and Surface Functionalized Glass, Alexander Dubček University of Trenčín, 911 50 Trenčín, Slovakia

[§]Catalonia Institute for Energy Research (IREC), Jardins de les Dones de Negre 1, 08930 Sant Adrià de Besòs, Barcelona, Spain

[∥]Helmholtz-Zentrum Berlin für Materialien und Energie, Hahn-Meitner-Platz 1, 14109 Berlin, Germany

[⊥]European Synchrotron Radiation Facility (ESRF), 71 Avenue des Martyrs, 38043 Grenoble, France

[#]Felix-Bloch-Institut für Festkörperphysik, Universität Leipzig, Linnéstraße 5, 04103 Leipzig, Germany

[▽]Instituto de Ciencia de Materiales de Madrid (CSIC), Cantoblanco, 28049 Madrid, Spain

[○]Institut für Geologische Wissenschaften, Freie Universität Berlin, Malteserstrasse 74-100, 12249 Berlin, Germany

S *Supporting Information*

ABSTRACT: The presence of Ge during the synthesis of thin film kesterite $Cu_2ZnSnSe_4$ (CZTSe) solar cell absorbers boosts their power conversion efficiency, especially due to an improved open circuit voltage. The mechanism underlying this beneficial effect of Ge is still under debate. We gained deep insights into the role of Ge by applying advanced synchrotron nanoprobe-based X-ray fluorescence spectroscopy and X-ray absorption near-edge structure spectroscopy to cross-sectional lamellas taken from high efficiency devices. We observe that Ge remains in the CZTSe absorber layer after the synthesis process with a specific heterogeneous distribution. Different grains contain different Ge concentrations. Moreover, Ge depletion exists at random grain boundaries but not at symmetric Σ3-boundaries, leading to different band alignments. The incorporated Ge occupies Sn lattice sites in the CZTSe crystal structure; however, the concentration is only 0.1 to 0.5 at %. Also Ge aggregates in nanoscale inclusions, which we could identify to be GeO_2 that likely lessen the beneficial effect of Ge on the photovoltaic performance.

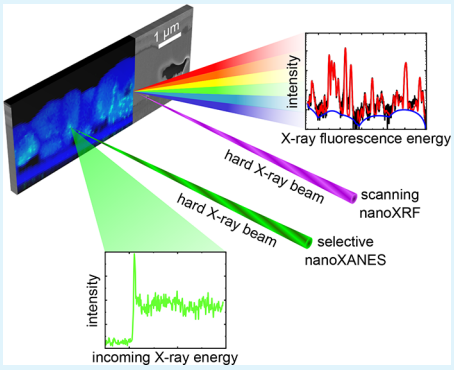

KEYWORDS: *kesterite, Ge-doping, thin-film photovoltaics, nanoXRF, nanoXANES*

INTRODUCTION

Kesterite materials, such as $Cu_2ZnSnSe_4$ (CZTSe), have drawn increasing attention for thin film solar cell applications because of their earth abundant, nontoxic constituents and their direct band gap of around 1 eV.[1] Compared to other thin film solar cells like $Cu(In,Ga)Se_2$ (CIGSe) or CdTe, the interest in kesterite solar cells is quite recent. Therefore, the conversion efficiency is still limited and reaches a record efficiency of only 12.6%.[2] This limitation is mainly attributed to losses in the open circuit voltage (V_{OC}) in relation to the optical band gap. The cause of this effect is not completely understood yet, and a number of reasons have been proposed, including potential fluctuations of the local composition, the formation of secondary phases, and/or the poor quality of the hetero-junctions.[3] Also the short minority carrier lifetime, originating from deep defects in the bulk or at grain boundaries, can be detrimental to the performance. Especially the multivalent characteristic of Sn with its ability to form +II and +IV oxidation states is predicted to be one of the essential problems of this material, as Sn^{2+} creates deep recombination centers, contributing to the poor open circuit voltage.[4−6]

To address this problem, CZTSe can be alloyed with Ge, which substitutes Sn. Such a Ge incorporation does not only widen the band gap from 1.00 eV up to 1.35 eV, but it also decreases the open circuit voltage deficit, most likely by suppressing the limiting Sn^{2+} states.[7−9] Recently, it has been shown that even small amounts of Ge drastically enhance the open circuit voltage without significantly affecting the band gap energy.[6] The most remarkable V_{OC} increase was found for 7.5 to 12.5 nm thick Ge layers deposited during the solar cell

Received: September 12, 2019
Accepted: December 3, 2019
Published: December 3, 2019

DOI: 10.1021/acsaem.9b01784
ACS Appl. Energy Mater. 2020, 3, 558−564

synthesis, resulting in a voltage increase from about 400 mV for Ge-free absorbers to values around 490 mV for Ge-containing ones.[10]

The beneficial effect of these small amounts of Ge is not completely understood yet, but so far a variety of suggestions were made to explain the boost in the open circuit voltage, including improved grain growth and morphology. Germanium can act as a fluxing agent and helps to modify the reaction pathways of CZTSe from a trimolecular process toward a mainly bimolecular process one.[6,11] Additionally, other factors like the superior control of the Na content in the absorber layer and at the interfaces or the improved charge transport properties might also increase the efficiency.[12−14]

To get further insights into the presence and role of Ge in CZTSe solar cells, we investigated high efficiency solar cells doped with Ge during fabrication. We use high spatial resolution X-ray fluorescence analysis (nanoXRF) to prove the Ge localization in the absorber and complementary electron microscopy techniques to correlate the Ge distribution with microstructural elements. Our findings reveal a Ge depletion at random grain boundaries, while highly symmetrical Σ3 twin grain boundaries are not affected. In addition, high spatial resolution X-ray absorption near-edge structure spectroscopy (nanoXANES) allows us to locally probe the atomic environment of Ge, showing the incorporation in the crystal structure of CZTSe but also the formation of small GeO_2 inclusions.

EXPERIMENTAL SECTION

The CZTSe:Ge solar cells were fabricated using a sequential process by sputtering Cu/Sn/Cu/Zn metallic stacks onto Mo-coated soda-lime glass. This process included the thermal evaporation of very thin Ge layers of 10 nm (at the top) and 5 nm (at the bottom) in order to dope the CZTSe, followed by the reactive annealing under an Se + Sn atmosphere (for details see the Supporting Information). The obtained conversion efficiency was 8.5% for the cell with Cu/(Sn+Zn) and Zn/Sn ratios of 0.77 and 1.19 and 7.6% for the cell with Cu/(Sn+Zn) and Zn/Sn ratios of 0.83 and 1.13. Cross-sectional lamellas were prepared out of the solar cells using a focused ion beam (FIB) in a FEI Helios NanoLab 600i DualBeam system, in the same way as described by Schöppe et al. in refs 15 and 16. For each CZTSe stoichiometry, two lamellas were prepared at different lateral positions. Additionally, cross-sectional lamellas were also made out of a commercial crystalline Ge wafer and a homogeneous, single-phase $Cu_2ZnGeSe_4$ (CZGSe) powder (grain size: ∼200 × 100 μm^2) synthesized by solid state reaction.[17] The final thicknesses of the lamellas ranged from 160 to 260 nm.

Scanning electron microscopy (SEM) and scanning transmission electron microscopy (STEM) were also applied using the FEI Helios NanoLab 600i DualBeam system. The STEM measurements were performed in partial high angle annular dark field (pHAADF) and dark field (DF) geometry. Bright field transmission electron microscopy (TEM) measurements were carried out using a JEOL JEM-3010. nanoXRF and nanoXANES were both conducted at the nanoanalysis beamline ID16B of the European Synchrotron Radiation Facility (ESRF) in Grenoble, France.[18] The measurements were performed using a two-step principle. In the first step, nanoXRF measurements (spot analyses and mapping) were conducted at the lamella. Therefore, the energy of the synchrotron nanobeam was set to 29.6 keV in "pink-beam" mode with an average photon flux of 2.5 × 10^{10} photons/s and a focal spot size of 54 × 52 nm^2 measured by gold knife edge scans.[18] The lamellas were raster scanned through the highly focused hard X-ray synchrotron nanobeam with a step size of 50 nm in vertical and horizontal directions. At each position, a full spectrum of the emitted X-ray fluorescence radiation was recorded by two 3-element silicon drift detectors with a counting time of 800 ms, keeping the dead time below 20%. The recorded spectra contain information about all elements of interest, i.e., Cu, Zn, Sn, Se, and Ge. By fitting the respective spectra using PyMCA,[19] the concentration for each element can be estimated. The impact of light alkalis on the absorber could not be quantified, since the fluorescence of any element lighter than Ar is absorbed by the air and the detector windows. In the second step, nanoXANES data were acquired in "monochromatic beam" mode (using a Si(111) double crystal monochromator) at the Ge edge (∼11.103 keV) with a focal spot size of about 150 × 135 nm^2 and an average photon flux of 1.4 × 10^7 photons/s. The energy was scanned with a step size of 1 eV to cover the range from 53 eV below to 197 eV above the Ge edge. The emitted fluorescence radiation was recorded by a Canberra X-PIPS SXD 7 element detector. For every energy, the counting time was 100 ms. Twenty scans were collected and summed up to obtain good statistics. Five such spectra were averaged to obtain the final XANES spectrum. Finally, the data were standardized, including partially smoothing within the normalization. Electron backscatter diffraction (EBSD) analyses were performed using a Jeol JSM 7600F SEM equipped with a Nordlis Max EBSD camera. EBSD scans were performed using a voltage of 20 kV and a current of up to 2.2 nA. The scans were captured using the Oxford Instruments software Aztec 3.1 and evaluated using the Channel 5 software package. Although the kesterite-type CZTSe is a tetragonal phase, the lattice parameters of a = 5.698 Å and c = 11.352 Å[20] complicate the EBSD analysis. The value of 2a is 11.396 Å causing a $c/2a$ relation of 0.996, i.e., kesterite-type CZTSe only shows a minimal tetragonal distortion. A similar problem occurs when attempting to analyze tetragonal ZrO_2 using EBSD; this case has been described in detail by Martin et al.[21] In the present case, the applied software failed to index the EBSD patterns obtained from the lamellas when supplying the available kesterite-type CZTSe material file based on ICSD-file no. 200419 but showed good indexing results when supplying a material file of cubic Si. As the options of influencing the indexing process, e.g., by deactivating specific reflectors, are limited in the applied software package, all EBSD scans were performed using only the material file of cubic Si. As a consequence of this cubic-approximation of the tetragonal crystal structure, the determined twinning relations are defined as 60° rotations around the ⟨111⟩ direction and as 70.53° rotation around the ⟨110⟩ direction in the approximated cubic structure instead of 60° rotations around the ⟨221⟩ direction and as 70.53° rotation around the ⟨110⟩ direction in the tetragonal lattice (for more details on the EBSD measurements see the Supporting Information).

RESULTS AND DISCUSSION

Figure 1a shows the SEM micrograph of the cross section of a Ge-doped CZTSe:Ge solar cell with Cu/(Sn+Zn) and Zn/Sn ratios of 0.83 and 1.13, respectively. The Mo back contact onto which the CZTSe:Ge absorber was grown is visible at the bottom of the micrograph. A thin $MoSe_2$ layer is formed between the Mo and the CZTSe:Ge during the selenization process. The CZTSe:Ge absorber is covered by a thin CdS buffer, an i-ZnO layer, and an indium tin oxide (ITO) front contact. The following protective Pt layer was deposited during the lamella preparation.[15,16] The absorber features voids with lateral sizes up to 1 μm, especially close to the back contact. They likely originate from Cu out-diffusion toward the surface while Zn diffuses to the back contact during the solar cell synthesis.[11,22] Figure 1b depicts the corresponding Ge intensity map, obtained by fitting the XRF spectrum for each pixel individually with PyMCA.[18] Ge can be identified inside the absorber, but it also seems to be visible on top of the solar cell. However, the latter does not originate from Ge but from Pt, because the Pt L2M1-line (L_η) partly overlaps with the Ge K-lines (see the Supporting Information).

Detecting the Ge signal in the CZTSe absorber grains clearly points to the Ge incorporation into the grains during the solar

DOI: 10.1021/acsaem.9b01784
ACS Appl. Energy Mater. 2020, 3, 558−564

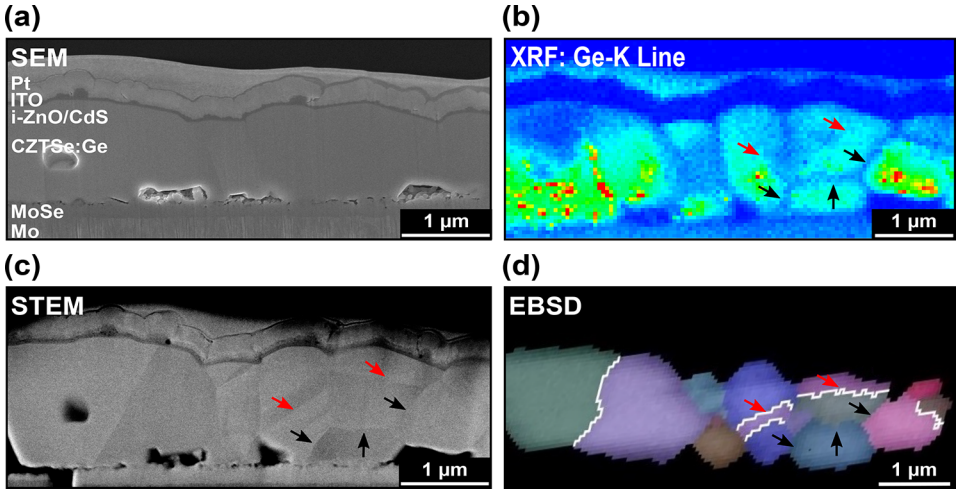

Figure 1. Microstructure and Ge distribution of the lamella taken out of a CZTSe:Ge solar cell with a Cu/(Sn+Zn) ratio of 0.83 and a Zn/Sn ratio of 1.13. (a) SEM image of the lamella. (b) Fitted Ge intensity map measured by nanoXRF and evaluated with PyMCA. The signal in the Pt layer originates from the Pt L_η line, which partly overlaps with the Ge K-lines. The red arrows indicate grain boundaries with a relatively homogeneous Ge intensity, while the black arrows point to grain boundaries with Ge depletion. (c) STEM-pHAADF image revealing different grain boundaries in the absorber layer. (d) BC+all Euler map, measured by EBSD, depicting the Euler angles of the different grains. The highly symmetrical Σ3 twin boundaries are marked by white lines.

cell synthesis. This is in contrast to a previous study where Ge was only detected as small nanoscale inclusions at specific grain boundaries using electron energy-loss spectroscopy,[23] likely due to the limited sensitivity of that method. In the same way, secondary ion mass spectrometry (SIMS) studies revealed that Ge tends to remain in the top-half part of the absorber but not in the bottom half.[6] However, the results presented in Figure 1b clearly show a heterogeneous Ge distribution throughout the grains. Distinct Ge intensity variations are present in the absorber. We find Ge hotspots, areas with a quite even distribution and areas with a Ge depletion. Opposite to the SIMS results, we observe a generally higher Ge concentration at the bottom half of the absorber (toward to the back contact) compared to the top half. Nevertheless, we also identified a few regions showing a similarly high Ge intensity near the front contact. To understand the reasons for these differences, p-HAADF STEM measurements in Figure 1c reveal the different layers of the solar cell and also the grain boundaries of the polycrystalline absorber (see the Supporting Information). The grain sizes fluctuate from 0.3 to 1.5 μm in diameter. Clearly, the Ge variations are related to different grains and their boundaries. Despite significant variations from grain to grain, single grains display mainly an even Ge concentration independent of their size. A significantly lower Ge content is visible at grain boundaries, though only certain grain boundaries are affected. In order to evaluate this behavior, the same lamella was scanned by EBSD to determine the orientation of the grains and the characteristics of the grain boundaries. High quality Kikuchi patterns were obtained from the absorber (see the Supporting Information), allowing reliable EBSD scans. Figure 1d shows the resulting all Euler map superimposed by the band contrast (BC) map, depicting the angles of the different grain orientation (for the BC +inverse pole figure (BC+IPF) map see thte Supporting Information). Highly symmetrical Σ3 twin grain boundaries (in this case all with a 60°-$\langle 111 \rangle_c$ misorientation) are highlighted by white lines. In the analyzed area, 70.53°-$\langle 110 \rangle_c$ grain boundaries were not observed. EBSD is fairly surface sensitive (the information depth is less than 100 nm in the applied setting[24]) in comparison to hard X-rays from the synchrotron source, which probes the whole 160 nm thick lamella. Hence not all grain boundaries are visible in the BC +all Euler map. Nevertheless, the observed random grain boundaries perfectly correlate with a Ge depletion, whereas the Ge intensity is unaffected for all Σ3 twin boundaries. The red arrows represent grain boundaries with a relatively homogeneous intensity and the presence of twin boundaries, while the black arrows specify random grain boundaries with Ge depletion. The only exception is observed on the right side of Figure 1b. Here, the Ge signal is decreased also for a Σ3 twin boundary. We assume that this is an incoherent Σ3 twin boundary. The Σ3 twins are basically stacking faults, thus, the grain growth is not affected, and the Ge incorporation continues in the same way as before. However, random grain boundaries are formed when a growth front encounters a second growth front with a different orientation, leading to a stop in growth and to the observed Ge depletion. We assume that the latter occurs, because the growth front is Ge poor. Germanium is incorporated with a time delay and partly exchanges Sn. It might also be possible that it occupies Sn vacancies or forms interstitials.

The Ge atomic concentration in the absorber grains was deduced by fitting the respective XRF spectra averaged over 9 pixels by PyMCA. The concentration ranges from about 0.1 at % to 0.5 at % and agrees well with the integral Ge concentration estimated from the amount of Ge introduced during the sequential synthesis process. Other studies have shown that the Ge introduction widens the band gap from 1.0 eV for 0 at % to 1.35 eV for 12.5 at %.[9] Thus, assuming a mostly linear behavior, the band gap in this sample enlarges by about 15 meV at most at 0.5 at % Ge content. Therefore, the nearly unaffected band gap is in excellent agreement with previous photoluminescence and external quantum efficiency measurements.[6,10] This finding corroborates that the enhanced conversion efficiency cannot be attributed only to a wider band gap.

Besides the overall band gap, the local band alignment can also impact the conversion efficiency. The detected Ge

DOI: 10.1021/acsaem.9b01784
ACS Appl. Energy Mater. 2020, 3, 558−564

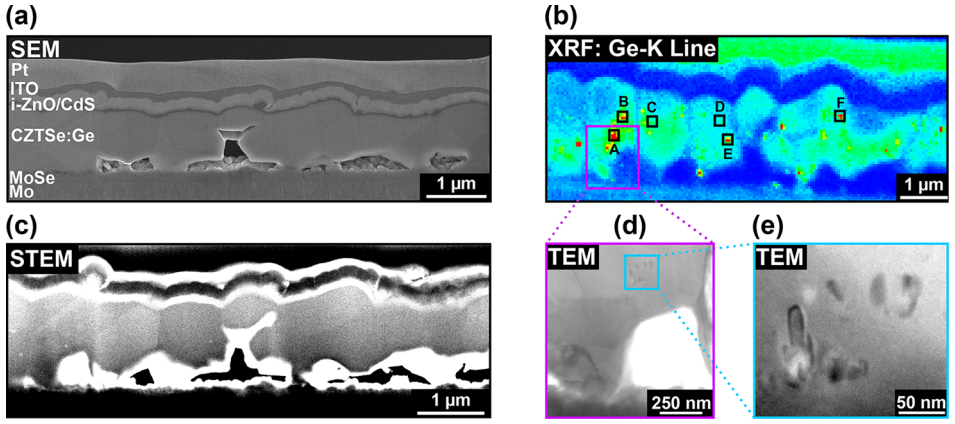

Figure 2. Microstructure and Ge distribution of the lamella taken out of a CZTSe:Ge solar cell with a Cu/(Sn+Zn) ratio of 0.77 and a Zn/Sn ratio of 1.19. (a) SEM image of the lamella with a thickness of 260 nm. (b) Fitted Ge intensity map measured by nanoXRF and evaluated with PyMCA. The black squares (A−F) mark the regions where nanoXANES measurements were performed. (c) STEM-DF image revealing different grain boundaries in the absorber layer. (d) TEM image taken in an area where Ge hotspots are observed. For this purpose, the lamella was thinned down to approximately 80 nm. (e) The magnified image corresponds to area A in panel (b) and clearly shows the formation of small nanoscale inclusions.

depletion at random grain boundaries slightly increases the energy of the valence band maximum, while the conduction band minimum is nearly unaffected, leading to an attractive force for the electrons toward the grain boundaries.[25] Since these random and incoherent grain boundaries most likely feature dangling and wrong bonds, acting as recombination centers, the Ge depletion at grain boundaries probably slightly lessens the overall beneficial effect of Ge.

The nanoXRF data were collected on four lamellas taken from two different CZTSe:Ge stoichiometries. Figure 2 represents the results taken on the cell with the higher conversion efficiency of 8.5% and with Cu/(Sn+Zn) and Zn/Sn ratios of 0.77 and 1.19, respectively. Similar to the previous findings, the lamella consists of the same layer stack and also shows voids in the absorber. The Ge distribution depicted in Figure 2b also reveals identical features. Different intensities for individual grains and an even Ge content within single grains are visible. Ge depletion in regions correlating with selected grain boundaries (Figure 2c) and Ge hotspots are observed as well. The other two lamellas (not shown) exhibit the same features, and we therefore conclude that these features represent general characteristics of Ge-doped CZTSe absorbers grown as described above.

The hotspots might either be secondary phases or Ge rich $Cu_2Zn(Sn,Ge)Se_4$ inclusions. In order to obtain more details from the detected Ge hotspots, TEM images were taken in the respective areas. Therefore, the lamella was thinned down to approximately 80 nm. Figures 2d and 2e illustrates TEM micrographs of an area with Ge hotspots recorded using different magnifications. The formation of small nanoscale inclusions with sizes between 10 and 50 nm is evident. Similar features were also observed in previous reports with slightly smaller diameters (1−10 nm).[6,10] However, in these studies most of the inclusions were concentrated around the CZTSe:Ge grain boundaries with only a few of them found embedded within large grains,[6] whereas here the inclusions are only present within the grains.

The estimated Ge concentration in an area of 2 × 2 pixels in the XRF map is up to 1.8 at % for the inclusions. According to the TEM results in Figure 2e, the inclusion size is 10−50 nm, thus, we can assume that the nanoscale inclusions are not present over the whole thickness of the lamella. By calculating the fraction of both volumes (see the Supporting Information), the actual Ge concentration of the inclusions can be considered to be about 20 at % or even higher, which is a strong indication of the presence of small secondary phases with higher Ge content rather than Ge rich $Cu_2Zn(Sn,Ge)Se_4$ inclusions.

Two recent articles have reported on the formation of Sn enriched nanoscale inclusions with dimensions similar to those reported here.[6,23] Thus, we evaluated the distribution of Sn (see the Supporting Information) and all other absorber elements, but no evidence of agglomeration or depletion in the XRF maps was found.

Since secondary phases can potentially limit the conversion efficiency of the solar cells and nanoXRF provides no information about the chemical bonding, nanoXANES data were collected to study the local Ge environment at the identical CZTSe:Ge lamella, which was already presented in Figure 2, for both the nanoscale inclusions and CZTSe:Ge grains. The black squares in Figure 2b roughly mark the regions (A−F) where the nanoXANES data were taken: (i) regions C and D correspond to the CZTSe:Ge absorber grains, and (ii) regions A, B, E, and F refer to the nanoscale Ge rich inclusions. Figure 3a presents the normalized nanoXANES spectra for regions C and D of the CZTSe:Ge grains compared to a homogeneous CZGSe reference. The latter lamella was prepared out of a homogeneous single phase CZGSe powder.[17] The spectral shape of the nanoXANES data for CZTSe:Ge grains and CZGSe is in good agreement and suggests that Ge occupies tetravalent Ge^{4+} sites in the CZTSe matrix of the absorber grains. Moreover, the XANES edge position gives further insights into the local coordination. The inset in Figure 3a shows the position of the edge energy of all spectra relative to the CZGSe reference, ΔE, evaluated at $\mu(E) = 0.5$. Within this analysis uncertainty of 0.3 eV for the edge energy, both investigated grains match the CZGSe reference. Thus, Ge is incorporated into the kesterite matrix on substitutional Sn lattice sites. Such a substitutional behavior is usually associated with the suppression of the +II oxidation state and therefore with the reduction of deep recombination centers for the photoexcited electrons.[4,7] However, as the maximum Ge concentration is only 0.5 at % in the present case compared to $Cu_2Zn(Sn,Ge)Se_4$ alloys, it is unlikely that this has a major

DOI: 10.1021/acsaem.9b01784
ACS Appl. Energy Mater. 2020, 3, 558−564

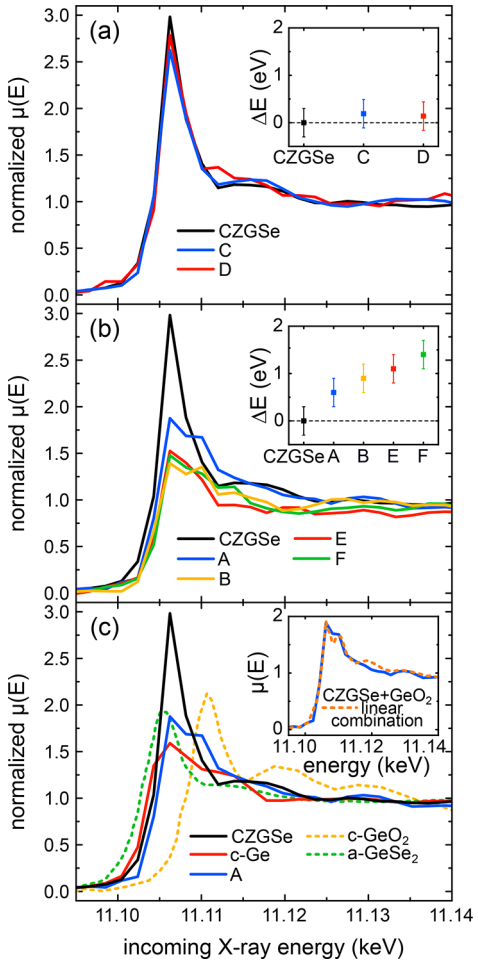

Figure 3. Normalized nanoXANES spectra measured at the Ge K-edge in different regions of the CZTSe:Ge lamella, which is displayed in Figure 2. (a) Normalized absorption coefficient $\mu(E)$ versus incoming X-ray energy for two positions of the CZTSe:Ge absorber layer (C and D as shown in Figure 2b) and the CZGSe reference lamella. (b) Normalized nanoXANES spectra measured at four different Ge hotspots (A, B, E, and F as shown in Figure 2b) compared to CZGSe. The insets in (a) and (b) plot the shift of the edge position relative to the CZGSe reference, ΔE, evaluated at $\mu(E) = 0.5$. (c) Normalized nanoXANES spectra for region A, the CZGSe reference lamella, and a crystalline Ge reference lamella together with normalized XANES spectra for crystalline GeO_2 taken from Ward et al.[26] and amorphous $GeSe_2$ taken from Zhou et al.[27] The inset plots the spectra for region A and for a linear combination of 60% CZGSe and 40% GeO_2.

impact on the improved open circuit loss, because the number of exchanged atoms is too small. Thus, there must be other reasons for the improved efficiency, such as a higher crystalline quality.[6,10,12,23]

Regions A, B, E, and F in Figure 2b contain Ge rich nanoscale inclusions. Compared to the CZTSe:Ge grains, the respective normalized nanoXANES spectra shown in Figure 3b clearly depict a different shape, different edge energy, and varying height of the white line, suggesting an additional contribution in the local structure of the nanoscale inclusions apart from the kesterite matrix. The inset of Figure 3b plots the shift of the edge energy position up to 1.4 eV relative to the CZGSe reference. Even by taking both the analysis uncertainty (0.3 eV) and the energy resolution of the Si (111) double crystal monochromator (1 eV) into account, no agreement with the CZGSe reference is apparent. Accordingly, three out of four regions fulfill the criterium of a shift ≥1 eV, supporting the assumption of the presence of a secondary phase.

The spectra were compared to suited reference materials to distinguish the additional contribution in the evaluated areas. Exemplarily, Figure 3c shows the normalized nanoXANES spectra for region A, for the CZGSe reference lamella, and for a crystalline Ge reference lamella together with normalized XANES spectra for crystalline GeO_2 taken from Ward et al.[26] and amorphous $GeSe_2$ taken from Zhou et al.[27] Because XANES is sensitive to the short-range structural order, within this energy range the spectra of the crystalline and the amorphous Ge phases are pretty similar, as shown in Backman et al.[28] NanoXANES is still very challenging today using a nanofocalization device at 165 m from the source and a fixed-exit Si (111) double crystal monochromator located at 35 m from the undulator. In addition, there were relatively low statistics during our measurements due to the low photon flux and sample thickness. Therefore, Figure 3c only shows the XANES spectra for the crystalline Ge reference.

The depicted references do not fit well with the data for region A. In particular, Ge and $GeSe_2$ compounds present lower absorption edge energies compared to the investigated cases (−0.4 eV shift for elemental Ge and −1.7 eV for $GeSe_2$ with respect to the CZGSe reference), thus, both materials can be excluded from the analysis (see Figure 3c). In principle, the ratio between Ge and Se can vary, producing a shift in the XANES edge. However, Zhou et al. showed that the absorption edge for $Ge_xSe_{(1-x)}$ (for $0.2 \leq x \leq 0.4$) is always below the one for amorphous Ge and that the composition dependent energy shift is quite small.[27] Therefore, independent of the chemical composition, we also exclude $Ge_xSe_{(1-x)}$ as a possible phase in our nanoscale inclusions.

The remaining GeO_2 reference also shows no obvious agreement with region A or any other region containing nanoscale inclusions. However, TEM observations in Figure 2e reveal maximum sizes between 10 and 50 nm for the inclusions, supporting our assumption that the inclusions are not present over the whole lamella thickness. Moreover, the X-ray beam dimensions used in the nanoXANES acquisitions were about 150 × 135 nm^2 (which is nearly three times larger than the maximum dimensions of the inclusions). The measured local structure should thus be a superposition of the kesterite CZTSe:Ge matrix with an unknown phase. Because GeO_2 is the only phase with a significant edge shift to higher energies, it was used with the CZGSe reference in a linear combination to describe the nanoXANES spectra of regions A, B, E, and F. The inset in Figure 3c representatively shows the resulting combination for 60% CZGSe and 40% GeO_2 compared to the spectrum of region A. The good agreement indicates that the nanoscale inclusions are very likely GeO_2. The same result was also found for the three other regions containing Ge hotspots but with different compound fractions. In addition, we performed nanoXANES measurements also on the other CZTSe:Ge solar cell lamellas and could confirm that all findings described above are independent of the stoichiometry.

Regarding the impact of these GeO_2 inclusions on the electrical properties of the absorber and the resulting solar cell devices, several parameters should be taken into account: the band gap, the electron affinity, and the carrier concentration. First, considering the wide band gap, about 5.7 eV,[29−31] and the very low electron affinity (2.24 eV[32]) compared to the

DOI: 10.1021/acsaem.9b01784
ACS Appl. Energy Mater. 2020, 3, 558−564

kesterite absorber material, these GeO_2 nanoparticles would locally create a barrier for the electrons. Nevertheless, considering the small size of the particles (<50 nm) compared to the carrier diffusion length and their local distribution throughout the absorber, they should not have a strong impact on the electrical transport properties since the electrons could easily circumvent these inclusions, although their contribution as potential recombination centers cannot be ruled out. Further investigations are needed regarding the carrier concentration level in these particles to confirm whether they could be acting as effective recombination centers or not. In any case, these particles in the CZTSe:Ge absorber will not effectively contribute to the light conversion; therefore, it might be beneficial to avoid or minimize their presence. On the other hand, the possible effect on the optical properties of the layer could be neglected due to the size, local distribution, and the relatively low concentration of particles. In addition, we performed nanoXANES measurements also on the other CZTSe solar cell lamellas and could confirm that all findings described above are independent of the stoichiometry.

CONCLUSION

The composition and local structure of high efficiency CZTSe solar cells was investigated by nanoXRF, nanoXANES, and different electron microscopy techniques. We show that Ge remains in the absorber after the solar cell synthesis, revealing a laterally inhomogeneous incorporation. The Ge distribution correlates with the presence of different grains, selected grain boundaries, and nanoscale inclusions. The Ge concentration varied between different grains, ranging from 0.1 to 0.5 at %, while for the inclusions a minimum concentration of 20 at % was estimated. In addition, our results show that random grain boundaries are Ge poor, leading to an attractive force for electrons and most likely to an increase of carrier recombination. The evaluation of the short-range structural order for Ge within the grains indicates that Ge occupies tetravalent Ge^{4+} sites, substituting Sn in the kesterite type crystal structure of CZTSe. Because of such small quantities of Ge within the grains, the band gap is not significantly widened, thus, we assume that this exchange is not the origin of the improved V_{OC}. Our findings prove the presence of GeO_2 nanoscale inclusions. They could limit the conversion efficiency because of the higher band gap and larger interface area, where electrons could eventually recombine.

ASSOCIATED CONTENT

Supporting Information

The Supporting Information is available free of charge at https://pubs.acs.org/doi/10.1021/acsaem.9b01784.

Details on solar cell synthesis and experimental methods, estimated compositions of investigated solar cells with their electrical data, Kikuchi patterns, BC+all Euler map and BC+IPF map, STEM-pHAADF image of lamella as shown in Figure 1, Sn intensity map of lamella as shown in Figure 2, and volume calculation of secondary phases (PDF)

AUTHOR INFORMATION

Corresponding Author

*Phone: +49 3641 947335. E-mail: maurizio.ritzer@uni-jena.de. Web site: https://www.photovoltaik.uni-jena.de.

ORCID

Maurizio Ritzer: 0000-0002-8202-7236
Philipp Schöppe: 0000-0001-9988-6232
Sergio Giraldo: 0000-0003-4881-5041
Edgardo Saucedo: 0000-0003-2123-6162
Carsten Ronning: 0000-0003-2667-0611

Notes

The authors declare no competing financial interest.

ACKNOWLEDGMENTS

The authors acknowledge the ESRF for provision of synchrotron radiation facilities (experiment: MA-3564) and the valuable help of Dr. Damien Salomon and Dr. Jaime Segura-Ruiz. This work was financially supported by the German Federal Ministry of Education and Research under the nano@work project (contract number: 05K16SJ1) and by the Deutsche Forschungsgemeinschaft (DFG, German Research Foundation) under the project number SCHN 1283/2-1. Support from the Spanish Ministry MINECO, "Generalitat de Catalunya" AGAUR and H2020 Programme is gratefully acknowledged through grants ENE2016-80788-C5-1-R, ENE2017-87671-C3-1-R, BES-2014-068533, 2017-SGR-862, and H2020-NMBP-03-2016-720907. Furthermore, this paper is a part of dissemination activities of project FunGlass, which has received funding from the European Unionś Horizon 2020 research and innovation programme under grant agreement No. 739566.

REFERENCES

(1) Ahn, S.; Jung, S.; Gwak, J.; Cho, A.; Shin, K.; Yoon, K.; Park, D.; Cheong, H.; Yun, J. H. Determination of band gap energy (Eg) of Cu2ZnSnSe4 thin films: On the discrepancies of reported band gap values. *Appl. Phys. Lett.* **2010**, *97*, 021905.

(2) Wang, W.; Winkler, M. T.; Gunawan, O.; Gokmen, T.; Todorov, T. K.; Zhu, Y.; Mitzi, D. B. Device Characteristics of CZTSSe Thin-Film Solar Cells with 12.6% Efficiency. *Adv. Energy Mater.* **2014**, *4*, 1301465.

(3) Siebentritt, S.; Schorr, S. Kesterites-a challenging material for solar cells. *Prog. Photovoltaics* **2012**, *20*, 512−519.

(4) Biswas, K.; Lany, S.; Zunger, A. The electronic consequences of multivalent elements in inorganic solar absorbers: Multivalency of Sn in Cu2ZnSnS4. *Appl. Phys. Lett.* **2010**, *96*, 201902.

(5) Kolmakov, A.; Potluri, S.; Barinov, A.; Menteş, T. O.; Gregoratti, L.; Niño, M. A.; Locatelli, A.; Kiskinova, M. Spectromicroscopy for addressing the surface and electron transport properties of individual 1-d nanostructures and their networks. *ACS Nano* **2008**, *2*, 1993−2000.

(6) Giraldo, S.; Neuschitzer, M.; Thersleff, T.; López-Marino, S.; Sánchez, Y.; Xie, H.; Colina, M.; Placidi, M.; Pistor, P.; Izquierdo-Roca, V.; Leifer, K.; Pérez-Rodríguez, A.; Saucedo, E. Large Efficiency Improvement in Cu 2 ZnSnSe 4 Solar Cells by Introducing a Superficial Ge Nanolayer. *Adv. Energy Mater.* **2015**, *5*, 1501070.

(7) Greenwood, N. N.; Earnshaw, A. *Chemistry of the elements*, 2nd ed.; Butterworth-Heinemann: Oxford, 1997; DOI: 10.1016/C2009-0-30414-6.

(8) Collord, A. D.; Hillhouse, H. W. Germanium Alloyed Kesterite Solar Cells with Low Voltage Deficits. *Chem. Mater.* **2016**, *28*, 2067−2073.

(9) Morihama, M.; Gao, F.; Maeda, T.; Wada, T. Crystallographic and optical properties of Cu 2 Zn(Sn 1−x Ge x)Se 4 solid solution. *Jpn. J. Appl. Phys.* **2014**, *53*, No. 04ER09.

(10) Giraldo, S.; Thersleff, T.; Larramona, G.; Neuschitzer, M.; Pistor, P.; Leifer, K.; Pérez-Rodríguez, A.; Moisan, C.; Dennler, G.; Saucedo, E. Cu 2 ZnSnSe 4 solar cells with 10.6% efficiency through

DOI: 10.1021/acsaem.9b01784
ACS Appl. Energy Mater. 2020, 3, 558−564

innovative absorber engineering with Ge superficial nanolayer. *Prog. Photovoltaics* **2016**, *24*, 1359−1367.
(11) Giraldo, S.; Saucedo, E.; Neuschitzer, M.; Oliva, F.; Placidi, M.; Alcobé, X.; Izquierdo-Roca, V.; Kim, S.; Tampo, H.; Shibata, H.; Pérez-Rodríguez, A.; Pistor, P. How small amounts of Ge modify the formation pathways and crystallization of kesterites. *Energy Environ. Sci.* **2018**, *11*, 582−593.
(12) Giraldo, S.; Neuschitzer, M.; Placidi, M.; Pistor, P.; Perez-Rodriguez, A.; Saucedo, E. Cu 2 ZnSnSe 4 -Based Solar Cells With Efficiency Exceeding 10% by Adding a Superficial Ge Nanolayer: The Interaction Between Ge and Na. *IEEE J. Photovoltaics* **2016**, *6*, 754−759.
(13) Neuschitzer, M.; Marquez, J.; Giraldo, S.; Dimitrievska, M.; Placidi, M.; Forbes, I.; Izquierdo-Roca, V.; Pérez-Rodriguez, A.; Saucedo, E. Voc Boosting and Grain Growth Enhancing Ge-Doping Strategy for Cu 2 ZnSnSe 4 Photovoltaic Absorbers. *J. Phys. Chem. C* **2016**, *120*, 9661−9670.
(14) Hages, C. J.; Levcenco, S.; Miskin, C. K.; Alsmeier, J. H.; Abou-Ras, D.; Wilks, R. G.; Bär, M.; Unold, T.; Agrawal, R. Improved performance of Ge-alloyed CZTGeSSe thin-film solar cells through control of elemental losses. *Prog. Photovoltaics* **2015**, *23*, 376−384.
(15) Schöppe, P.; Schnohr, C. S.; Oertel, M.; Kusch, A.; Johannes, A.; Eckner, S.; Burghammer, M.; Martínez-Criado, G.; Reislöhner, U.; Ronning, C. Improved Ga grading of sequentially produced Cu(In,Ga)Se 2 solar cells studied by high resolution X-ray fluorescence. *Appl. Phys. Lett.* **2015**, *106*, 013909.
(16) Schöppe, P.; Gurieva, G.; Giraldo, S.; Martínez-Criado, G.; Ronning, C.; Saucedo, E.; Schorr, S.; Schnohr, C. S. Discrepancy between integral and local composition in off-stoichiometric Cu 2 ZnSnSe 4 kesterites: A pitfall for classification. *Appl. Phys. Lett.* **2017**, *110*, 043901.
(17) Gurieva, G.; Többens, D. M.; Valakh, M. Y.; Schorr, S. Cu-Zn disorder in Cu 2 ZnGeSe 4: A complementary neutron diffraction and Raman spectroscopy study. *J. Phys. Chem. Solids* **2016**, *99*, 100−104.
(18) Martínez-Criado, G.; Villanova, J.; Tucoulou, R.; Salomon, D.; Suuronen, J.-P.; Labouré, S.; Guilloud, C.; Valls, V.; Barrett, R.; Gagliardini, E.; Dabin, Y.; Baker, R.; Bohic, S.; Cohen, C.; Morse, J. ID16B: a hard X-ray nanoprobe beamline at the ESRF for nano-analysis. *J. Synchrotron Radiat.* **2016**, *23*, 344−352.
(19) Solé, V. A.; Papillon, E.; Cotte, M.; Walter, P.; Susini, J. A multiplatform code for the analysis of energy-dispersive X-ray fluorescence spectra. *Spectrochim. Acta, Part B* **2007**, *62*, 63−68.
(20) Valle Rios, L. E.; Neldner, K.; Gurieva, G.; Schorr, S. Existence of off-stoichiometric single phase kesterite. *J. Alloys Compd.* **2016**, *657*, 408−413.
(21) Martin, S.; Berek, H.; Aneziris, C. G.; Martin, U.; Rafaja, D. Pitfalls of local and quantitative phase analysis in partially stabilized zirconia. *J. Appl. Crystallogr.* **2012**, *45*, 1136−1144.
(22) Fairbrother, A.; Fontané, X.; Izquierdo-Roca, V.; Espíndola-Rodríguez, M.; López-Marino, S.; Placidi, M.; Calvo-Barrio, L.; Pérez-Rodríguez, A.; Saucedo, E. On the formation mechanisms of Zn-rich Cu2ZnSnS4 films prepared by sulfurization of metallic stacks. *Sol. Energy Mater. Sol. Cells* **2013**, *112*, 97−105.
(23) Thersleff, T.; Giraldo, S.; Neuschitzer, M.; Pistor, P.; Saucedo, E.; Leifer, K. Chemically and morphologically distinct grain boundaries in Ge-doped Cu 2 ZnSnSe 4 solar cells revealed with STEM-EELS. *Mater. Des.* **2017**, *122*, 102−109.
(24) Wisniewski, W.; Saager, S.; Böbenroth, A.; Rüssel, C. Experimental evidence concerning the significant information depth of electron backscatter diffraction (EBSD). *Ultramicroscopy* **2017**, *173*, 1−9.
(25) Shu, Q.; Yang, J.-H.; Chen, S.; Huang, B.; Xiang, H.; Gong, X.-G.; Wei, S.-H. Cu 2 Zn(Sn,Ge)Se 4 and Cu 2 Zn(Sn,Si)Se 4 alloys as photovoltaic materials: Structural and electronic properties. *Phys. Rev. B: Condens. Matter Mater. Phys.* **2013**, *87*, 115208.
(26) Ward, M. J.; Rupar, P. A.; Murphy, M. W.; Yiu, Y.-M.; Baines, K. M.; Sham, T. K. Ionic nature of Ge(II)-centered dications: a germanium K-edge X-ray absorption near edge structures study. *Chem. Commun. (Cambridge, U. K.)* **2010**, *46*, 7016−7018.
(27) Zhou; Paesler; Sayers. Structure of germanium-selenium glasses: An x-ray-absorption fine-structure study. *Phys. Rev. B: Condens. Matter Mater. Phys.* **1991**, *43*, 2315−2321.
(28) Backman, M.; Djurabekova, F.; Pakarinen, O. H.; Nordlund, K.; Araujo, L. L.; Ridgway, M. C. Amorphization of Ge and Si nanocrystals embedded in amorphous SiO2 by ion irradiation. *Phys. Rev. B: Condens. Matter Mater. Phys.* **2009**, *80*, 144109.
(29) Atuchin, V. V.; Kaichev, V. v.; Korolkov, I. v.; Saraev, A. A.; Troitskaia, I. B.; Perevalov, T. v.; Gritsenko, V. A. Electronic Structure of Noncentrosymmetric α-GeO 2 with Oxygen Vacancy: Ab Initio Calculations and Comparison with Experiment. *J. Phys. Chem. C* **2014**, *118*, 3644−3650.
(30) Ramana, C. V.; Carbajal-Franco, G.; Vemuri, R. S.; Troitskaia, I. B.; Gromilov, S. A.; Atuchin, V. V. Optical properties and thermal stability of germanium oxide (GeO2) nanocrystals with α-quartz structure. *Mater. Sci. Eng., B* **2010**, *174*, 279−284.
(31) Sevik, C.; Bulutay, C. Theoretical study of the insulating oxides and nitrides: SiO2, GeO2, Al2O3, Si3N4, and Ge3N4. *J. Mater. Sci.* **2007**, *42*, 6555−6565.
(32) Zhou, M.; Shao, L.; Miao, L. Matrix Isolation Infrared Spectroscopic and Density Functional Theoretical Calculations of the GeO 2- and GeO 4- Anions. *J. Phys. Chem. A* **2002**, *106*, 6483−6486.

DOI: 10.1021/acsaem.9b01784
ACS Appl. Energy Mater. 2020, 3, 558−564